Thermal Neutron Scattering Cross Sections for Graphitic Amorphous Carbon

T. Ahmed[1], N. C. Fleming[2], and A. I. Hawari[3]

Nuclear Reactor Program, Department of Nuclear Engineering, North Carolina State University, Raleigh, NC 27695, USA

[1]tahmed4@ncsu.edu, [2]ncsorrel@ncsu.edu, [3]ayman.hawari@ncsu.edu

ABSTRACT

Carbon materials are commonly found in both nuclear reactors and experimental systems. Various carbon structures occur in nuclear applications ranging from crystalline and nuclear graphite to the amorphous carbon seen in next-generation advanced reactor designs. Amorphous carbon is based on a randomized graphite-like structure and offers the unique ability to disperse impurities throughout the bulk composition. A graphite-like amorphous carbon system was modeled using the classical molecular dynamics (MD) code LAMMPS (Large-scale Atomic/Molecular Massively Parallel Simulator). An improved version of the temperature-dependent Adaptive Intermolecular Reactive Empirical Bond Order (AIREBO) potential was used to model the carbon-carbon atomic interactions for the temperature at 300 K along with densities 1.60, 1.70, 1.85, and 2.23 g/cm^3. From the normalized velocity autocorrelation function (VACF), the phonon density of state (DOS) was then calculated as the Fourier transform of the normalized VACF. This DOS was then used as the primary input for the evaluation of the thermal scattering law (TSL, i.e. $S(\alpha,\beta)$) and associated neutron thermal scattering cross sections. The TSL was analyzed using the Full Law Analysis Scattering System Hub (*FLASSH*). The amorphous structure results in shifts of the phonon DOS to lower energy modes than typically displayed for ideal crystalline graphite. This impact on the DOS is directly reflected in the TSL. Furthermore, the typical features and the optical graphitic peak at 0.25 eV for the ideal graphite DOS disappear for graphite-like amorphous carbon, which shows good agreement with the expected structure.

1. INTRODUCTION

Carbon materials are vital moderators in a nuclear reactor and include numerous pyrolytic and reactor grade forms. The reactor grade graphite is made from petroleum or pitch cokes and comprises crystalline graphite granules embedded in an amorphous binder carbon matrix. As the name suggests, reactor-grade graphite is designed for use in nuclear power generation [1-2]. It also has crystalline regions that are embedded in amorphous carbon. The average density of amorphous carbon is typically 1.60 to 1.85 g/cm^3 and is lower than that of perfect graphite [1,3]. All amorphous carbon has a disorder structure. However, numerous variations of the structure have been discovered, and the characteristics of these variants vary greatly depending on the manufacturing specifics.

The graphite-like (sp^2) to diamond-like (sp^3) binding ratio is used to classify types of amorphous carbon. The existence of any hydrogen in the system and the density are essential variables that affect the binding properties. The sp^2 to sp^3 binding ratio is, in fact, strongly linked to the density and stress of synthesis. A higher percentage of sp^2 binding is correlated to a lower density and/or stress [4-5]. Therefore, for this study, densities of 1.60, 1.70, 1.85, and 2.23 g/cm^3 were used at 300 K, which is lower than the density of ideal graphite (nearly 2.25 g/cm^3) [1,6]. Some of the earlier research on amorphous carbon was investigated based on primarily tetrahedral (ta-c) or diamond-like carbon and amorphous graphene [7-9]. However, few atomic modeling investigations of low-density graphitic amorphous carbon phases have been conducted so far [1,10]. Those simulations were based on an in-house MD code at North Carolina State University (NCSU), explicitly developed for graphite and graphitic amorphous carbon studies and tight-binding molecular-dynamics (TBMD), respectively.

While there have been many computational molecular dynamics (MD) investigations on carbon materials, comparatively few have been on amorphous carbon. However, because of its great fitting database and thorough consideration of coordination effects, the semiempirical many-body reactive bond order (REBO [11]) potential has proved very common for modeling carbon material structures. It is impossible to maintain the layered structure of graphite above the above-ground state. Therefore, the REBO potential needs to be supplemented by a supplemental expression reflecting nonbonded interplanar interactions. The adaptive interatomic REBO potential (AIREBO), introduced by Stuart et al. [12], incorporates a Lennard-Jones potential into the REBO formulation to account for long-range forces. This Lennard-Jones (LJ) term in the carbon material's potential increases the number of interacting pairs, significantly contributing to graphite interlayer interactions. This approach is taken into consideration in the papers [1-2, 12] for crystalline and amorphous graphite simulation.

In nuclear research, the neutron scattering cross sections are needed to describe neutron thermalization. To evaluate the thermal scattering cross section, the material density of states (DOS) is required, and this can be developed directly from MD simulations [1-2]. From the normalized velocity auto correlation function (VACF), the phonon DOS was calculated as the Fourier transform of the VACF. This DOS was then used as the primary input for the evaluation of the thermal scattering law (TSL, i.e. $S(\alpha,\beta)$) and associated neutron thermal scattering cross sections. In this paper, we present an atomic model of graphitic amorphous carbon at the above-mentioned densities at 300 K temperature using LAMMPS [13-14] MD package in combination with VMD [15] and *FLASSH* [16] software. This methodology allows for direct validation of the material simulation and therefore a high fidelity TSL.

2. COMPUTATIONAL METHODOLOGY

Rather than the original AIREBO [12] potential, this MD model is based on a temperature dependent improved AIREBO potential initiated by Hehr [1].

In general, the AIREBO potential adds the following three terms:

$$E = \frac{1}{2}\sum_i \sum_{j\neq i}[E^{REBO} + E^{LJ} + E^{TORSION}] \quad (1)$$

where E^{REBO}, E^{LJ}, and $E^{TORSION}$ describe the REBO [11], LJ contributions, and torsional influences, respectively. The REBO potential is expressed as:

$$E^{REBO} = f_c(r_{ij})\left[V_R(r_{ij}) + b_{ij}V_A(r_{ij})\right] \quad (2)$$

Where V_A and V_R describe the attractive and repulsive force, respectively. For crystalline graphite atomic modeling [1], a temperature-dependent expansion coefficient, $C(T)$, was used to modify the magnitude of the attractive and repulsive contribution to the REBO potential described as:

$$V_R(r_{ij}) = A\left[1 + \frac{Q}{r}\right] e^{\left(-\alpha(r_{ij} - C(T)T)\right)} \quad (3)$$

$$V_A(r_{ij}) = \sum_{n=1}^{3} B_n e^{\left(\beta(r_{ij} - C(T)T)\right)} \quad (4)$$

Inside the LAMMPS [13-14] implementation, the temperature-dependent $A(T)$, and $B(T)$ are assigned at 300 K. The value of Q is 0.3363743908992296 Å such that the potential correctly predicted the phonon density of crystalline graphite.

The E^{LJ} the term was considered to have a weak temperature dependence and $E^{TORSION}$ term is omitted because it describes an explicit 4-body potential that defines various dihedral angle preferences in hydrocarbon configurations. Finally, the improved AIREBO potential was implemented on crystalline graphite to produce the best quality density of state at 300 K. Furthermore, and the improved AIREBO potential has been implemented on the graphitic amorphous carbon model along with densities 1.60, 1.70, 1.85, and 2.23 g/cm^3 at 300 K temperature. The initial configuration of this amorphous carbon atomic model has been generated from a cubic box that randomly contains 27,000 simple cubic carbon atoms. The box dimensions maintain the input density of the model. With a timestep of 0.5 fs, the model was heated to 9000 K for 100,000 timesteps (50 ps). The system was then cooled at a rate of 0.40 K/timesteps to the target temperatures at 300 K. Again, the system was equilibrated for another 50 ps using an NVT ensemble at the target temperatures at 300 K. The normalized velocity autocorrelation function (VACF) was then calculated over 2.5 ps. A total of 5,000 ps (2000 loops of 2.5 ps) was evaluated to obtain an accurate time averaged normalized VACF. In all the simulations, the periodic boundary condition (PBC) was used during the calculations to keep the particle number constant and eliminate the boundary effect. The atomic hybridizations are evaluated from the coordination number of each atom considering 1.825 Å cutoff and recorded at the end of a loop in the trajectory file. The radial distribution function (RDF), and the angular distribution functions (ADF), are calculated at every 50th timestep and averaged over each loop. The final RDF, ADF, and atomic hybridization are considered over the loop average. An in-house code is still under development to obtain the atomic hybridization for every timestep. The procedure is summarized in Fig. 1 below:

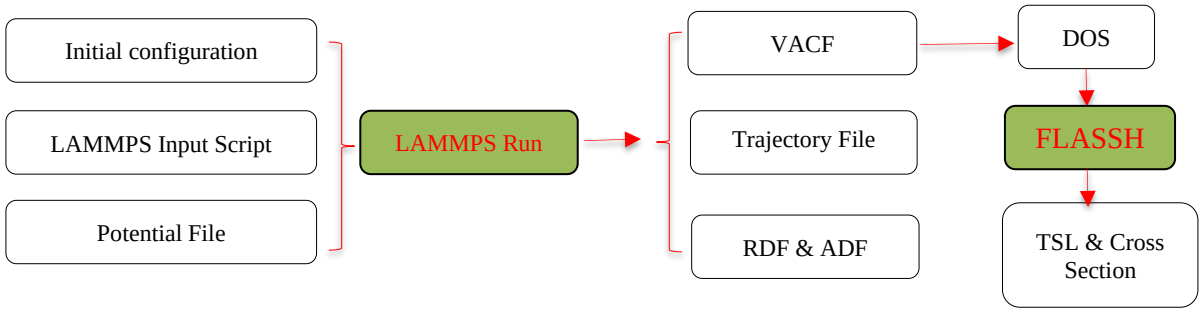

Figure 1. Summarized procedure of calculation process.

3. RESULTS AND DISCUSSIONS

The amorphous carbon constructed by the above-mentioned quenching method along with the density of 1.60, 1.70, 1.85, and 2.23 g/cm^3 at 300 K temperature is shown in Fig. 2. In this figure, it is visually clear that the system is well unstructured, which is created from the perfect random configuration. The visualization was done by VMD [15] software.

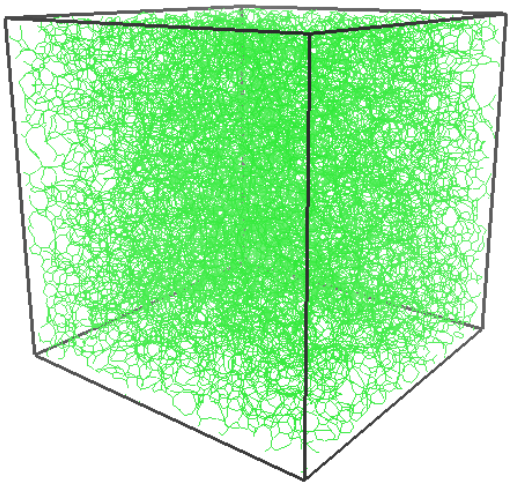

Figure 2. Atomic snapshot of a simulated configuration of the equilibrium graphitic amorphous carbon at a density of 1.60 g/cm^3 at 300 K.

In a system of atoms, the radial distribution function $g(r)$ describes how density varies as a function of distance from a reference particle. The radial distribution function, $g(r)$, is defined,

$$g(r) = \lim_{dr \to 0} \frac{p(r)}{4\pi(\frac{N_{pairs}}{V})r^2 dr} \tag{5}$$

where r is the distance between a pair of particles, $p(r)$ is the average number of atom pairs found at a distance between r and $r + dr$, V is the total volume of the system, and N_{pairs} is the number of unique pairs of atoms.

The first coordination number can be defined using the radial distribution function $g(r)$:

$$n_1(r) = 4\pi\rho_n \int_{r_0}^{r_1} r^2 g(r) dr \tag{6}$$

where $\rho_n = \frac{N_{pairs}}{V}$ is the number density, r_0 is the rightmost position starting from r = 0 Å whereon $g(r)$ is zero, r_1 is the first minimum position which is at r = 1.825 Å for the amorphous carbon atomic model for all densities at 300 K.

Fig. 3 shows the MD generated radial distribution function, $g(r)$, in black and the first coordination number $n_1(r)$ in red for graphite-like amorphous carbon in above mentioned four densities at 300 K. The position of the first peak of radial distribution function (RDF) is approximately 1.435 Å, which is consistent with the carbon bond length (1.421 Å) of crystalline graphite [17]. It is also noticed that the first peak height decreases with the increase of density, indicating the carbon atoms are well packed in the comparison of low density to high density. The area under the first peak of radial distribution function (RDF) is also presented in Fig. 3 for all densities at 300 K temperature. It is the measurement of the first coordination

number, $n_1(r)$ that indicates the number of neighboring atoms of a reference atom. In this atomic model, the average first coordination number is around three, which corresponds to the number of nearest neighboring carbon atoms of a reference carbon atom, indicating the sp^2 hybridization of the carbon atom dominates in this graphite-like amorphous carbon model for all densities at 300 K. This behavior is exceptionally dependent on the way of the amorphous carbon preparation procedure, especially on temperature and pressure.

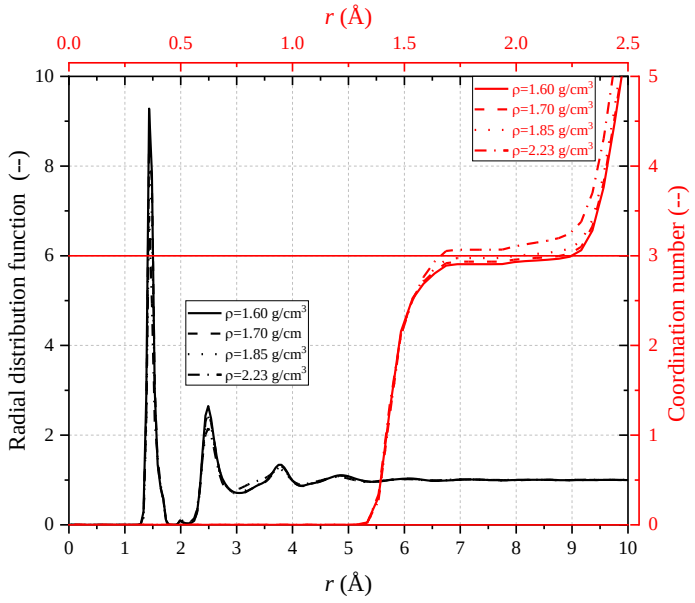

Figure 3. The radial distribution function and the coordination number of the equilibrium graphitic amorphous carbon at 300 K.

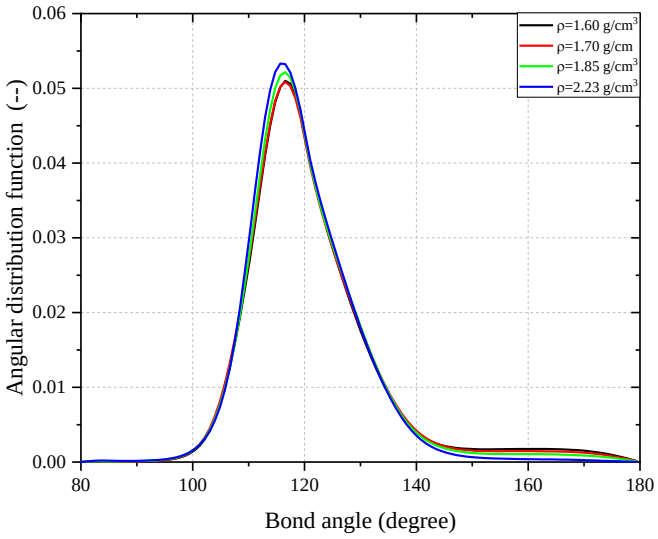

Figure 4. The angular distribution function of equilibrium graphitic amorphous carbon at 300 K.

The angular distribution function (ADF) is defined for angles between nearest neighbors carbon atoms in the amorphous system. In Fig. 4, the angular distribution function is shown for all densities at 300 K temperature. In this model, the bond angle of the carbon atom is around 116.55 degrees, close to the crystal graphite bond angle 120 degrees , indicating the sp^2 domination behavior. In Table I, the percentages of carbon atom hybridization are shown with previous published literature [18].

Table I. Percentage of sp^1, sp^2, and sp^3 hybridization

	1.6 g/cm^3	1.6 g/cm^3 [18]	1.7 g/cm^3	1.85 g/cm^3	2 g/cm^3 [18]	2.23 g/cm^3	2.50 g/cm^3 [18]
sp^1	13.1%	--	10.8%	8%	--	2.7%	--
sp^2	83%	89%	84.9%	86.5%	91.7%	87.8%	92.2%
sp^3	3.9%	1.8%	4.3%	5.5%	2.7%	9.5%	5.2%

The phonon density of state (DOS) describes the number of excitation states which the system may occupy. The VACF directly correlates the atomic motion in the graphitic amorphous carbon model to the available energy states. In this MD simulations, the general VACF is calculated from LAMMPS [13-14]. The normalized velocity autocorrelation function $C(t)$, is calculated as:

$$C(t) = \frac{\langle \boldsymbol{v}(t)\boldsymbol{v}(0)\rangle}{\langle \boldsymbol{v}(0)\boldsymbol{v}(0)\rangle}, \tag{7}$$

where $\boldsymbol{v}(t)$ represents the velocity at time t of carbon atom in the graphitic amorphous carbon. The density of state is the Fourier transform of the velocity autocorrelation function, $C(t)$ as:

$$\rho_s(\omega) = \int_{-\infty}^{\infty} C(t)e^{-i\omega t}dt, \tag{8}$$

where ω is phonon frequency (i.e. energy, $E = \hbar\omega$) [19].

Figure 5 represents the Normalized velocity autocorrelation function (VACF) for the equilibrium graphitic amorphous carbon along with the density of 1.60, 1.70, 1.85 and 2.23 g/cm^3 at 300 K temperature. It is noticed that in all cases, the normalized VACF is similar and shows few oscillation that confirm the low diffusion of carbon atom in this graphite-like amorphous carbon. The initial general VACF of this graphitic amorphous carbon is $\langle \boldsymbol{v}(0)\boldsymbol{v}(0)\rangle = \frac{3k_BT}{m} \approx 62.30$ Å^2/ps^2 which is the static limit in both cases, where k_B is the Boltzman constant, T is the system temperature, and m is the mass of carbon atom.

The average self-diffusion of the carbon atom in this atomic model, $D = \frac{1}{3}\int_0^{\infty}\langle \boldsymbol{v}(t)\boldsymbol{v}(0)\rangle dt$ is close to zero. This trivial diffusion process is indicative of solid materials. The phonon DOS of this atomic model of graphitic amorphous carbon is shown in Fig. 6 compared to MD model [1] and a set of neutron spectroscopy measurements on sputtered and glassy carbon samples [20] with the ideal crystalline ENDF/B-VIII.0 graphite [21]. The typical features of the phonon DOS of graphite-like amorphous carbon disappear from the optical graphitic peak at 0.25 eV shows good agreement with the expected structure [1,20]. The phonon DOS of sputtered amorphous carbon is comparatively dissimilar to the other DOS because it is dominated by sp^3 hybridization [22], where the glassy carbon is not dominated by the sp^3 hybridization. The glassy carbon, on the other hand, has a density of roughly 1.47 g/cm^3 which is lower than the average density of nuclear graphite and much lower than the density of the crystalline form [21]. When the graphitic amorphous carbon density is reduced from 2.23 to 1.6 g/cm^3, the DOS is significantly impacted which will directly translate into determining the cross sections of this system.

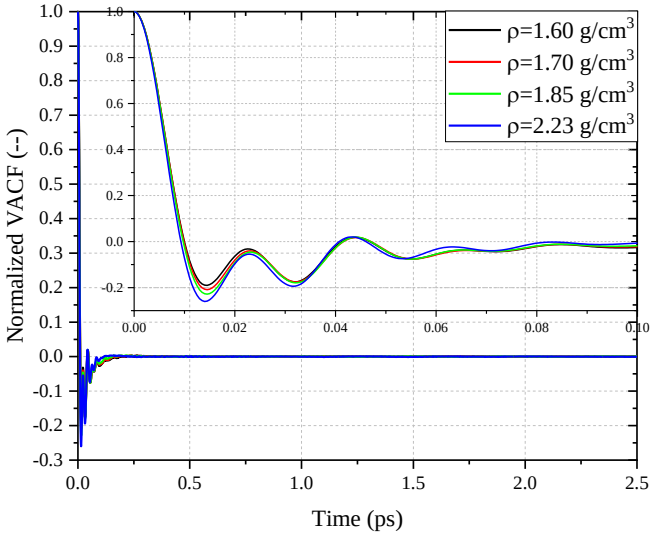

Figure 5. The normalized velocity autocorrelation function of the equilibrium graphitic amorphous carbon at 300 K.

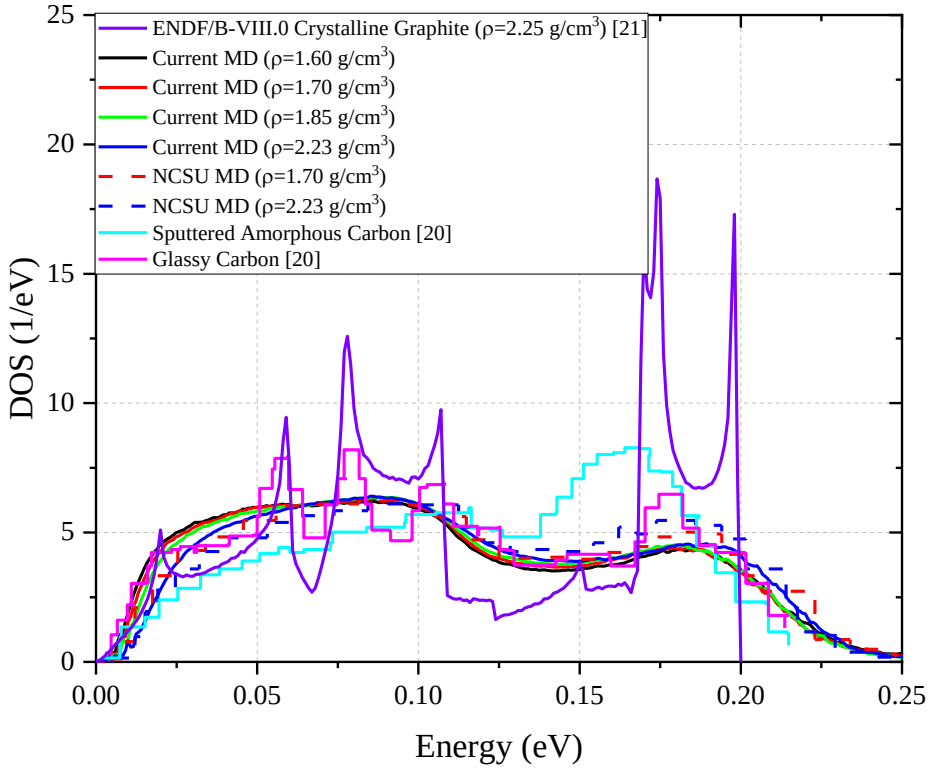

Figure 6. The density of state of the equilibrium graphitic amorphous carbon at 300 K.

The thermal neutron scattering cross sections were computed using the *FLASSH* code based on the phonon density of states provided above [16]. In this case, the double differential scattering cross section is expressed as:

$$\frac{d^2\sigma}{d\Omega dE} = \frac{\sigma_{coh}}{4k_BT}\sqrt{\frac{E\prime}{E}}e^{-\frac{\beta}{2}}S_s(\alpha,\beta), \tag{9}$$

where σ_{coh} is the bound atom coherent scattering cross section, E and E' represent the initial and final energies, respectively, of the neutron, and $S_s(\alpha,\beta)$ is the incoherent (or self) scattering law, which is directly dependent on the density of states $\rho(\omega)$ (see Ref. [6]). In addition, α and β represent dimensionless momentum and energy exchange variables respectively, and are given by $\alpha = \frac{E+E^{'}-2\sqrt{EE'}\mu}{Ak_BT}$ and $\beta = \frac{\hbar\omega}{k_BT}$, where A is atomic weight, and μ is the cosine of the scattering angle in the laboratory frame.

The resulting TSL for each density was evaluated at 300 K with only inelastic scattering contributions considered in the evaluation. An example of the TSL generated for the data with ρ=1.6 g/cm^3 is given in Fig. 7.

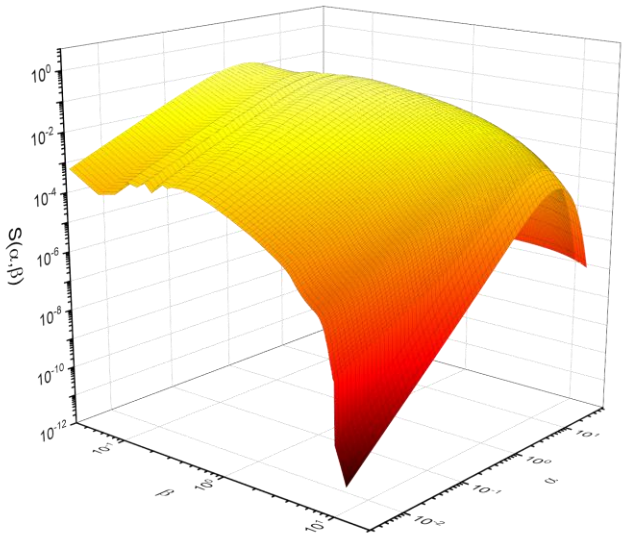

Figure 7. TSL for graphitic amorphous carbon at 300 K with a density of 1.6 g/cm^3.

Just as the features of the DOS are smoothed, the resulting TSL demonstrates a smooth surface without sharp features, reflecting the smooth structure seen in the DOS. Further, because amorphous carbon does not have a defined, regular crystalline structure, in the cross section elastic scattering will be minimized and only inelastic scattering will have significant contribution. The resulting scattering cross sections are given in Fig. 8. With increasing density, the cross sections decrease and approach that of the ideal crystalline ENDF/B-VIII.0 graphite. In the lowest energy region in particular, the impact of the graphite density is clearly seen. At higher energies, the disordered amorphous structure results in a consistently lower cross section than the ideal graphite [23]. Because of the higher energy modes and increased structure in ideal graphite, the inelastic cross section will more sharply increase to the free atom asymptote. For the amorphous structures, the DOSs are compressed to lower energies and as a result will have a lower cross section in the energy range from 1e-2 to the 5 eV asymptote.

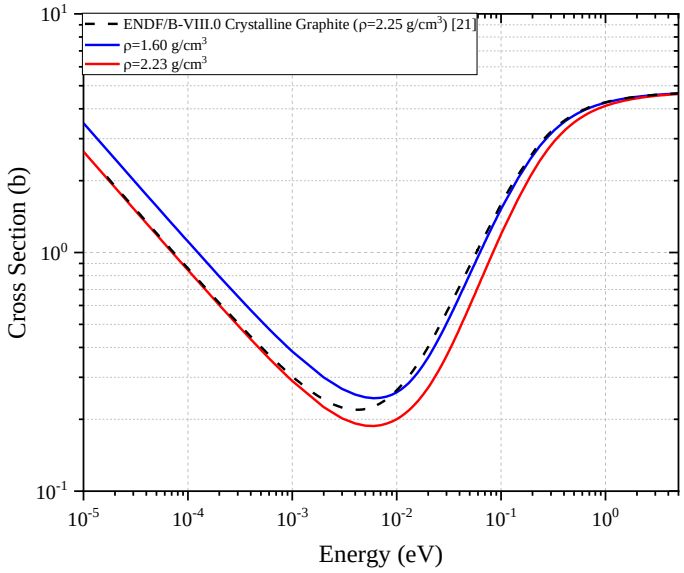

Figure 8. The thermal scattering cross sections of graphitic amorphous carbon at 300 K for various densities and compared with ideal crystalline graphite. .

4. CONCLUSIONS

A classical molecular dynamics simulation has been employed to compute the radial and angular distribution function, coordination number, atomic hybridization, velocity autocorrelation function, density of state, and the thermal neutron scattering cross section of graphitic amorphous carbon with the density of 1.60, 1.70, 1.85, 2.23 g/cm^3 at 300 K temperature. It is noticed that the density is significant in determining the structure and resulting cross sections for nuclear grade carbon. The thermal neutron scattering cross sections were estimated using the predicted phonon density of state and compared to other published data with a good agreement. The produced data may now be used in reactor physics benchmarks to improve neutronic simulation and quantify the reactivity impact.

REFERENCES

1. B.D. Hehr, *Development of the Thermal Neutron Scattering Cross Sections of Graphitic Systems using Classical Molecular Dynamics Simulations*, PhD Thesis, North Carolina State University, USA (2010).
2. B.D. Hehr, A.I. Hawari, and V.H. Gillette, "Molecular dynamics simulations of graphite at high temperatures," *Nuclear Technology* **160**(2), pp. 251-256 (2014).
3. C.R. Gould, A.I. Hawari, and E.I. Sharapov, "Re-Analysis of Recent Neutron Diffusion and Transmission Measurements in Nuclear Graphite," *Nuclear Science and Engineering* **165**(2), pp. 200-209 (2000).
4. D.G. McCulloch, D.R. McKenzie, and C.M. Goringe, "Ab Initio Simulations of the Structure of Amorphous Carbon," *Physical Review B* **61**(3), pp. 2349-2355 (2000).
5. J. Robertson, "Diamond-like Amorphous Carbon," *Materials Science and Engineering: R: Reports* **27**(4-6), pp. 129-281 (2002).
6. A.I. Hawari, and V.H. Gillete, "Inelastic Thermal Neutron Scattering Cross Sections for Reactor-Grade Graphite," *Nuclear Data Sheets* **118**, pp. 176-178 (2014).

7. D.A. Drabold, P.A. Fedders, and M.P. Grumbach, “Gap Formation and Defect States in Tetrahedral Amorphous Carbon,” *Physical Review B* **54**(8), pp. 5480-5484 (1996).
8. J. Dong, and D.A. Drabold, “Ring Formation and the Structural and Electronic Properties of Tetrahedral Amorphous Carbon Surfaces,” *Physical Review B*, **57**(24), pp.15591-15598 (1998).
9. Y. Li, and D.A. Drabold, Symmetry Breaking and Low Energy Conformational Fluctuations in Amorphous Graphene,” *Physica Status Solidi B* **250**(5), pp. 1012-1019 (2013).
10. C.Z. Wang, K.M. Ho, and C.T. Chan, “Tight-Binding Molecular-Dynamics Study of Amorphous Carbon,” *Physical Review Letters,* **70**(5), pp. 611-614 (1993).
11. D.W. Brenner, et. al., “A Second-Generation Reactive Empirical Bond Order (REBO) Potential Energy Expression for Hydrocarbons,” *Journal of Physics: Condensed Matter* **14**(44), pp. 783-801 (2002).
12. S.J. Stuart, A.B. Tutein, and J.A. Harrison, “A Reactive Potential for Hydrocarbons with Intermolecular Interactions,” *The Journal of chemical physics* **112**(14), pp. 6472-6486 (2000).
13. S. Plimpton, “Fast Parallel Algorithms for Short-Range Molecular Dynamics,” *Journal of computational physics* **117**(1), pp. 1-19 (1995).
14. “LAMMPS,” https://lammps.sandia.gov/.
15. “VMD,” http://www.ks.uiuc.edu/Research/vmd/.
16. N.C. Fleming, C.A. Manring, B.K. Laramee, et al., “*FLASSH* 1.0: Full Law Analysis Scattering System Hub,” *Transactions of the American Nuclear Society*, Washington, DC, November 30 - December 3 (2021).
17. S. Ergun, “Structure of Graphite,” *Nature Physical Science* **241**, pp. 65–67 (1973).
18. R. Ranganathan, S. Rokkam, T. Desai, and P. Keblinski, “Generation of Amorphous Carbon Models Using Liquid Quench Method: A Reactive Molecular Dynamics Study”, *Carbon*, **113**, pp. 87-99 (2017).
19. A. Rahman, M.J. Mandell, and J.P. McTague, “Molecular Dynamics Study of an Amorphous Lennard-Jones System at Low Temperature,” *The Journal of Chemical Physics* **64**(4), pp. 1564-1568 (1976).
20. W.A. Kamitakahara, “Dynamics of Li-carbon and Carbon Solids,” *Journal of Physics and Chemistry of Solids* **57**(6-8), pp. 671-676 (1996).
21. J.L. Wormald, and A.I. Hawari, “Thermal Neutron Scattering Law Calculations Using ab initio Molecular Dynamics,” *EPJ Web of conferences*, 146, 13002 (2017).
22. J. Robertson., “Diamond-like Amorphous Carbon,” *Materials Science and Engineering R*, **37**, pp. 129-281 (2002).
23. F.C. Cowlard, and J.C. Lewis, “Vitreous Carbon — A New Form of Carbon” *Journal of Materials Science*, **2**, pp. 507-512 (1967).